The Greater Cederberg–False Bay Large Igneous Province in South Africa: A southern node of widespread magmatism associated with South Atlantic rifting

C.G. Kingsbury
Department of Geology, University of Pretoria, Pretoria, South Africa
Faculty of Geology and Geography, Tomsk State University, Tomsk Russia
e-mail: TheCGKings317@gmail.com

W. Altermann
Chairman South African Committee for Stratigraphy and Freelance Consultant, Pretoria, South Africa
e-mail: altermannw@gmail.com

J. Kramers
Department of Geology, University of Johannesburg, Johannesburg, South Africa
e-mail: jkramers@uj.ac.za

R.E. Ernst
Faculty of Geology and Geography, Tomsk State University, Tomsk, Russia
Department of Earth Sciences, Carleton University, Ottawa, Canada
e-mail: RichardErnst@cunet.carleton.ca

U. Söderlund
Department of Geology, Lund University, Lund, Sweden.
e-mail: ulf.soderlund@geol.lu.se

M.B. Klausen
Department of Geology, Stellenbosch University, Stellenbosch, South Africa
e-mail: klausen@sun.ac.za

Abstract

A new 130 to 140 Ma mafic dyke swarm, is identified in western South Africa. It consists of the previously undated Cederberg dyke swarm (CDS), for which we report U-Pb ID-TIMS baddeleyite ages of 131.4 ± 4.5 Ma (Knersvlake subswarm) and 133.0 ± 1.5 Ma (Doring-Tanqua subswarm). $^{40}Ar/^{39}Ar$ dates on these two samples and two additional dates of the Doring – Tanqua subswarm cluster between 128.5 ± 1.4 Ma and 132.2 ± 1.5 Ma. We also report $^{40}Ar/^{39}Ar$ ages of 139.3 ± 3.5 Ma for an east-west trending dyke located further north: 27 km south of Kleinsee, and 140.3 ± 1.2 Ma for an east-west dyke near Garies. Together, these eight ages robustly date the emplacement of the northern part of a Greater Cederberg- False Bay Dyke Swarm (GCFDS) at *ca.* 130 to 140 Ma. Trace and rare earth element data

reported herein suggest these dykes are compositionally E-MORB basalts that underwent modification either via subduction-modified lithospheric mantle, or by continental crust, or a combination thereof, and are petrogenetically similar to the *ca.* 132 Ma False Bay dykes around Cape Town. Therefore, we propose to unify all these coeval and compositionally similar dykes into one large igneous province (LIP) termed the Greater Cederberg-False Bay Large Igneous Province (GCF-LIP).

Introduction

The opening of the South Atlantic Ocean has long been linked to the *ca.* 130 Ma Paraná-Etendeka LIP of South America and southwestern Africa (e.g. White and McKenzie, 1989). More recently, another node of *ca.* 130 Ma magmatism and rifting was recognised another 3 000 km to the north on the South American side, the Equatorial Atlantic Magmatic Province (EQUAMP) (Hollanda et al., 2019). This northern node of Cretaceous magmatism, EQUAMP, has since been renamed the Borborema LIP (BOR-LIP; Matos, 2021) on the basis of new findings that recognise that this northern node of magmatism is both larger in areal extent, and in overall duration (135 to 140 Ma) than what was previously known. A third potential (southern) node of 130 Ma magmatism and rifting can be found in western South Africa and includes a previously dated *ca.* 131 Ma False Bay Dyke Swarm (FBDS; Reid et al., 1991; Stewart et al., 1996), and an as yet undated Cederberg Dyke Swarm (CDS) along with a series of three east-west trending dykes to the north of the CDS. When referred to collectively, these three dyke swarms will be known as the Greater Cederberg – False Bay Dyke Swarm (GCFDS) based on results and information presented in this contribution.

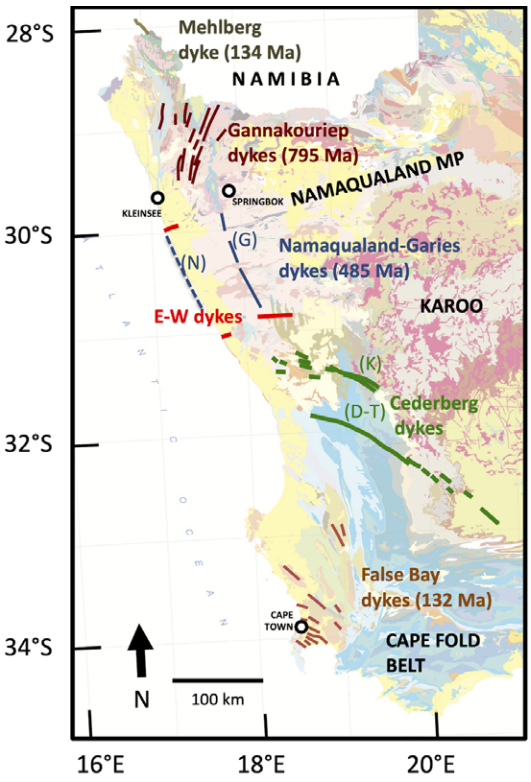

Figure 1. *Regional dyke distribution map of western South Africa. Base geology is from the Council for Geoscience (2019). Key to abbreviations as to subswarms or dykes: K=Knersvlakte; D-T=Doring-Tanqua (Naming from Trumbull et al., 2007); N=Namaqualand and G=Garies. The age of Melhberg is from Reid and Rex (1994), Gannakouriep is from Rioux et al. (2010), Namaqualand-Garies, Kingsbury et al. (2021) and False Bay from Reid et al. (1991).*

The setting of the southern node of *ca.* 130 Ma magmatism includes evidence of other large-scale magmatic events in the region between Cape Town and South Africa's frontier region with Namibia. These magmatic events consist of five broadly coast-parallel dyke swarms that represent large-scale magmatism active at different time intervals in Earth's history (Figure 1). From south to north, these swarms include the 132 Ma FBDS in the vicinity of Cape Town (Reid et al., 1991) the hitherto undated CDS, the *ca.* 485 Ma Namaqualand-Garies dykes (Kingsbury et al., 2021) and the *ca.* 795 Ma Gannakouriep dyke swarm just south of the Namibia boundary (Reid et al., 1991; Ransome, 1992; Rioux et al., 2010) and finally the 134 Ma Cretaceous Mehlberg dyke which extends into southernmost Namibia (Reid and Rex, 1994).

Herein, we focus on the CDS and investigate whether it could also be 130 Ma in age. As traced from Google Earth® imagery, the Cederberg mafic dyke swarm is characterised by two parallel, northwest trending subswarms (Figure 2). These northwest-trending subswarms are named the Knersvlakte dykes (northern, labeled "K" on Figure 2) and Doring-Tanqua (southern, labeled "D-T" on Figure 2) dykes by Trumbull et al. (2007) and separated from each other by *ca.* 50 km. Towards the south-east, Cederberg dykes generally cut 315 to 320° across the Neoproterozoic Namaqualand metamorphic province and form a broad arc, which becomes progressively west-trending, (*ca.* 270 to 290°) closer to the Atlantic coast. Furthermore, the CDS strikes parallel to the trend of the FBDS.

Age of Paraná-Etendeka LIP

Widespread Cretaceous dyke swarms and lava successions of *ca.* 134 Ma located in western South Africa, Namibia and Brazil have traditionally been viewed of as one single Paraná-Etendeka LIP (PE-LIP; Peate, 1997). As it stands, 11 separate U-Pb age determinations from zircons and baddeleyites from six Paraná lavas and five associated intrusions have revealed a tight clustering of ages (133.4 ± 0.2 Ma to 135.6 ± 1.8 Ma; Pinto et al., 2011; Janasi et al., 2011; Florisbal et al., 2014; Almeida et al., 2017), recording roughly 2 myr of magmatism within the South American part of the LIP. The Transminas dyke swarm of Brazil also records emplacement ages of *ca.* 130 Ma (Pessano et al., 2021 and references therein) while there remains a paucity of U-Pb ages for its conjugate African part. These age determinations

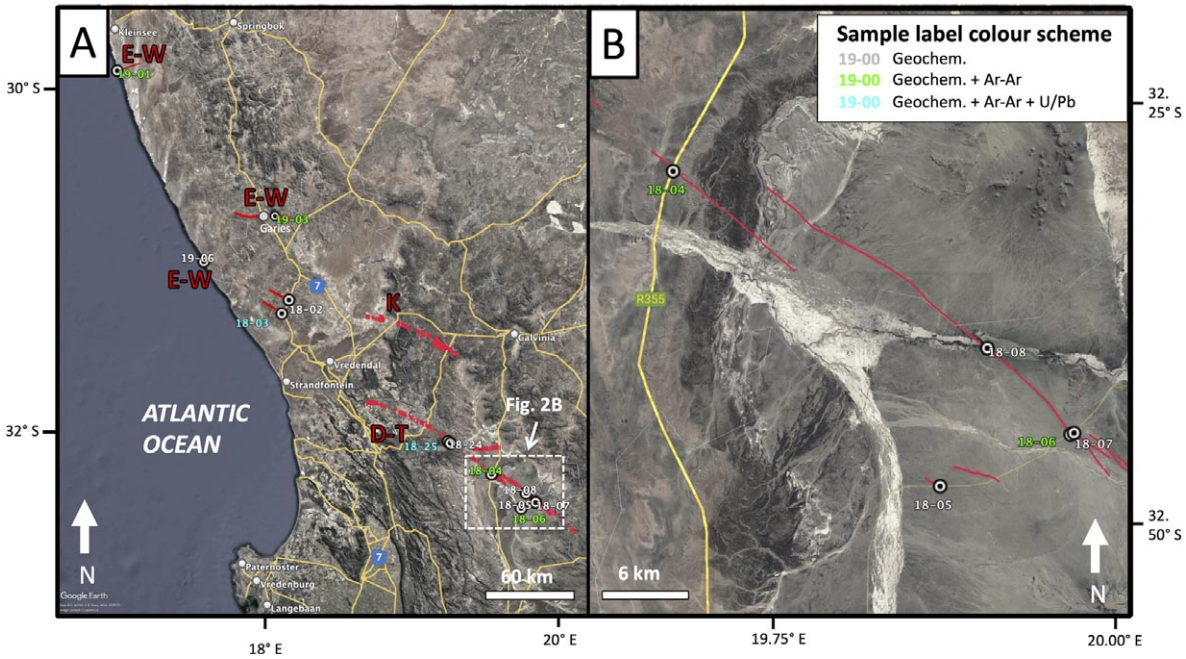

Figure 2. *Google Earth® imagery of the Cederberg and east-west dykes showing sample locations (**A**) regional map covering the full extent of the study area and (**B**) zoomed-in extent showing better resolution of sample collecting localities within white square in (A). In the interest of clarity, for this figure, sample identification numbers are shortened such that, for example "18 [CK 0]03" is read here as "18-03" with the numbers and letters between the brackets removed. Satellite data from USGS (Landsat), European Union (Copernicus), Airbus and Maxar Technologies.*

demonstrating a geologically short period of magmatism are further supported by a compilation of 67 Ar-Ar ages and 18 U-Pb ages, mostly from the Paraná (Brazil) sector, but some from the Etendeka (Namibia) sector (some duplicates), which strongly suggest a 135 to 133 Ma period of magmatism (Gomes and Vasconcelos, 2021 and references therein).

130 Ma magmatism south of the Paraná-Etendeka LIP

Farther to the south and along the African margin, $^{40}Ar/^{39}Ar$ geochronology constrains a 134 ± 3 Ma whole rock age for the Melhberg dyke (Reid and Rex, 1994), as well as a 131.3 ± 1.3 Ma plagioclase age for a False Bay Dyke (Stewart et al., 1996), supplemented by a composite K-Ar age of 132 ± 6 Ma for another False Bay Dyke (Reid et al., 1991). Apart from these scarce $^{40}Ar/^{39}Ar$ and K-Ar ages, further *ca.* 130 Ma magmatism along the southern African margin can only be inferred from geochemical linkages and dyke swarm trends (Reid et al., 1991; Trumbull et al., 2007; Backeberg et al., 2011). In this contribution, we remedy the paucity of ages as described above with U-Pb baddeleyite and additional $^{40}Ar/^{39}Ar$ ages, along with geochemical data that recognise and characterise additional 130 to 140 Ma dykes in South Africa.

Methods

Samples of dolerite were mainly collected alongside national and regional roads that intersect dykes, (Figure 2) previously mapped on a regional basis by the Council for Geosciences (2019; Figure 1). Suitable sampling sites were targeted on Google Earth®, although, in some cases these later were found unsuitable for geochronological and geochemical analyses due to extensive weathering, or a Quaternary alluvium cover.

U-Pb geochronology

Hand-specimens of sample 18CK003, -004 and -005 were sent to the University of Lund (Sweden) for baddeleyite extraction following the method developed by Söderlund and Johansson (2002). Of these samples, 18CK003 returned baddeleyite in quantities sufficient for U-Pb age determination. Sample 18CK025B was collected during a successive field campaign and, for this sample, separation was performed by electric pulse disaggregation using a SelFrag Lab® apparatus housed at the University of Pretoria. The sample was subject to repeat 120kV pulses inside a process vessel that was fitted with a 350 µm sieve. To reduce the risk of cross- contamination, the process vessel components were thoroughly washed with water prior to and after mineral liberation. The 350 µm-sieved separates were dried at 50°C and placed into a labeled plastic bag. Sample 18CK025B was sent to the University of Lund for baddeleyite extraction (Söderlund and Johansson, 2002).

Between three to nine grains for each fraction were transferred into Teflon dissolution bombs and washed repeatedly with two to three N nitric acid, including one *ca.* 20 minutes step on a hotplate at *ca.* 80 °C. A small amount of $^{236-233}U$-^{205}Pb tracer solution was added in each Teflon vial before being sealed and placed in a steel jacket. The baddeleyite grains were completely dissolved in HF:HNO_3 (10:1) at 180°C in the oven over three days. Each sample was loaded on an outgassed Re filament and

Pb and U isotopic ratios were measured on a Thermo Scientific Triton thermal ionisation multicollector mass spectrometer at the Museum of Natural History in Stockholm. The intensities of ^{207}Pb, ^{206}Pb, ^{205}Pb and ^{204}Pb were measured in dynamic (peak-switching) mode. A proxy value for Th/U for each fraction was obtained by reading off the intensities of ^{208}Pb and ^{206}Pb (in cps) after data acquisition was completed. Fractionation-corrected U isotopic ratios were determined by monitoring the deviation in ^{233}U/^{236}U with respect to the tracer solution (close to unity). The model composition of Stacey and Kramers (1975) was used to correct for initial common Pb. Total Pb and U blank were estimated at 0.5 and 0.05 pg. Decay constants used are from Steiger and Jäger (1977). Analytical results have been calculated and plotted using the Excel Add-in Isoplot (Ludwig, 2003).

Ar-Ar geochronology

Individual sub-millimeter grains of fine-grained matrix were irradiated as part of a stack of 60 samples in the B2W position of the Safari1 research reactor, operated by NTP Isotopes (pvt) Ltd, a subsidiary of the Nuclear Energy Corporation of South Africa (NECSA) at the Pelindaba Nuclear Research Centre, Gauteng, South Africa. The duration of irradiation was five hours for the 18CK samples (four samples), and ten hours (in a different batch) for the 19CK ones (three samples) with the reactor running at 20 MW. Aliquots of McClure Mountain hornblende reference material (523.1 ± 1 Ma, Renne et al., 1998) were interspersed in four positions with the samples. We acknowledge that certain studies question the utility of the McClure Mountain hornblende standard as a suitable Ar-Ar monitoring standard based on heterogeneity and reproducibility concerns (Baksi et al., 1996; Renne et al., 1998; Jiang et al., 2023). However, internal experience with this standard consistently yields stable Ca/K and Cl/K factors, paired with continuous monitoring of run-regressions, error propagations and uncertainties associated with J-values via internally developed software through Monte-Carlo simulations (e.g. Makhubela et al., 2017). Samples were analysed at the University of Johannesburg by stepwise heating using a defocused 1 064 nm wavelength beam from a Spectron ® continuous Nd-YAG laser. Heating steps, lasting five minutes each, started at *ca*. 500°C and increased until no more Ar was released, at *ca*. 1 400°C. A single collector MAP 215-50 noble gas mass spectrometer equipped with a Johnston electron multiplier (operated in analogue mode) was used. Pairs of SAES APG 10 getters (one kept at 450°C and one cold) are positioned in the extraction line as well as in the mass spectrometer adjacent to the ion source. Each analysis comprised seven cycles through all five Ar isotopes, with a run duration of 12 minutes, and data reduction was done using the aforementioned in-house program using linear and exponential fits of data, on each run, against time and extrapolating to time 0, when the gas is let into the mass spectrometer. Blanks were measured prior to analysis and interspersed after four consecutive heating steps in the sequence. Isotope fractionation was monitored though measuring air Ar from a 2.6 litre air reservoir at *ca*. 3E-2 mbar, and corrected for. Ages were calculated using the ^{40}K decay constant value $(5.541 \pm 0.014)\times10^{-10}$ a^{-1} (Kossert and Günther, 2004). Apart from ages, derived from the ^{40}Ar/^{39}Ar ratio, the isotope data also provide information on Ca/K (from ^{37}Ar/^{39}Ar) and Cl/K (from ^{38}Ar/^{39}Ar) respectively, calibrated on the McClure Mountain hornblende. The decay constants of ^{37}Ar, ^{39}Ar and ^{42}Ar used herein for calculation purposes are based on Stoenner et al. (1965) and Renne and Norman (2001).

Geochemistry

With the exception of samples 19CK001, -003 and -006 (outlined below), sample preparation for geochemistry was performed at the University of Pretoria's Stoneman Laboratory. Samples were individually crushed by jaw crusher to centimeter-sized fragments. Prior to the first run and between each sample run, the equipment was cleaned with alcohol, wiped vigorously and air-dried. A selection of sample crushes that contained no visual evidence of remnant surficial weathering was then pulverised in a tungsten carbide ring mill, which was also cleaned with alcohol, air-blast and wiped after each sample run. To further reduce contamination, silica sand was pulverised after each sample run in order to help dislodge potential previous sample remnants from the ring mill. The ring mill was again cleaned using alcohol, air-blast and wiping techniques. We acknowledge that there is potential for contamination in certain trace elements (e.g. Ta, Co and W) by using the tungsten carbide mill. However, studies (e.g., Yamasaki et al., 1998) along with laboratory experience (Lenhardt et al., 2023 and Lenhardt, writ. com) call into question a laboratory-induced contamination signal of Nb and Ta large enough to meaningfully impact petrogenetic interpretations. Also, as shown below our data exhibit a weak negative Nb anomaly, which suggests that Nb contamination is minimal. Powdered samples were ultimately divided into two aliquots of roughly equal volume each, sealed in labeled sample bags. Labeled powdered samples were delivered to ALS Geochemistry in Johannesburg (https://www.alsglobal.com/services-and-roducts/geochemistry) for geochemical analyses of major and trace elements. Major elements were analysed using ALS method code ME-ICP06. This method employs Inductively Coupled Plasma – Atomic Emissions Spectroscopy (ICP-AES). For this method, 0.100 g of sample is mixed and then subsequently fused in a furnace with a metaborate flux that then gets dissolved in 100 mL of 4% nitric acid and 2% hydrochloric acid before analyses. Trace elements including rare earth elements were analysed using ALS method code ME-MS81. In this procedure, a 0.100 g sample is mixed with a lithium borate flux, fused in a furnace, cooled and dissolved in a three-acid mixture of HNO_3, HCl and HF prior to analyses in an Inductively Coupled Plasma-Mass Spectrometer (ICP-MS). For samples 19-CK-001, -003 and -006, major elements were analysed via XRF at the Stoneman Lab (University of Pretoria) and trace elements were analysed via ICP-MS at Stellenbosch University. Details of methodologies and quality control for the three mentioned samples for geochemical analytical purposes are outlined in Kingsbury et al. (2021).

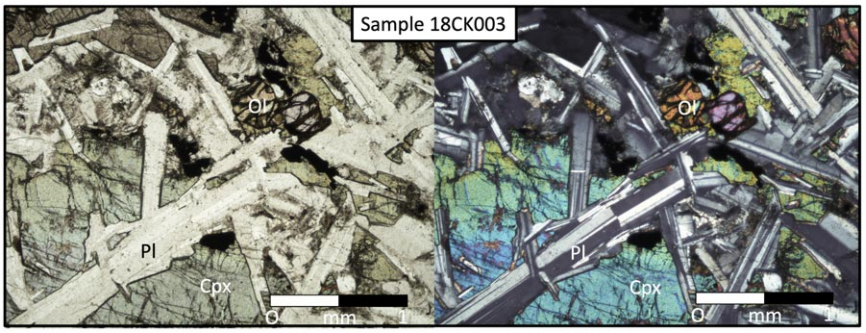

Figure 3. *Photomicrograph of Sample 18CK003 showing representative texture in plane-polar (left) and cross-polar (right). Key to abbreviations: Cpx=clinopyroxene; Ol=olivine and Pl=Plagioclase.*

Results

Petrography

Petrographic analysis reveals that the Cederberg dykes consist of mineral assemblages that are common for mafic dykes, i.e. plagioclase, clinopyroxene (augite) and occasionally olivine (Figure 3). No baddeleyite was observed in thin-section, likely due to the very small, micrometre-scale grain size. Mineral constituents were typically of 1 mm or less in size with a sub-ophitic texture. Samples varied from moderately altered (plagioclase alteration to clays) to near-pristine with no evidence of a metamorphic overprint.

U-Pb geochronology

Sample 18CK003 was collected from a dolerite dyke that measures ~90 m in width, strikes 305° (towards the northwest) and exhibits a sub-vertical dip. This dyke is part of the Knersvlakte (northern) sub-swarm of the Cederberg dykes that consists of three to four distinct dykes. The dyke is exposed in a roadcut along the R363, 26 km southwest from Nuwerus in the Western Cape (coordinates 31.356°S, 18.235°E; Figure 2). Sample 18CK025B was collected from a side-gully along the Biedouwrivier valley (coordinates 32.109°S, 19.381°E). The dyke in this location – the main dyke within the 2 to 4 dyke Doring-Tanqua (southern) subswarm – strikes 305° towards the northwest and is approximately 35 m wide based on Google Earth measurements. Approximately 30 baddeleyite grains, or fragments of grains, from each sample of 18CK003 and 18CK025B were recovered. The grains are up to *ca*. 150 µm in longest dimension, light brown and of excellent quality. We noticed a greater portion of unbroken grains in sample 18CK025B that was processed using the SelFrag Lab® apparatus. Two fractions of each sample, comprising three to nine grains per fraction, were selected for U-Pb ID-TIMS analysis (Appendix, Table 1). (Appendix data files are archived in the South African Journal of Geology repository (https://doi.org/10.25131/sajg126.0023.sup-mat)).

All fractions of samples 18CK003 and 18CK025B plot concordant and overlap within error (Figure 4). The two analyses of 18CK025B plot slightly to the right of the concordia curve yielding a relatively high MSWD value of 4.4 when calculated as a concordia age. We thus prefer the $^{206}Pb/^{238}U$ ages of 131.4 ± 4.5 and 132.8 ± 1.5 Ma to best date the crystallisation of these two dykes.

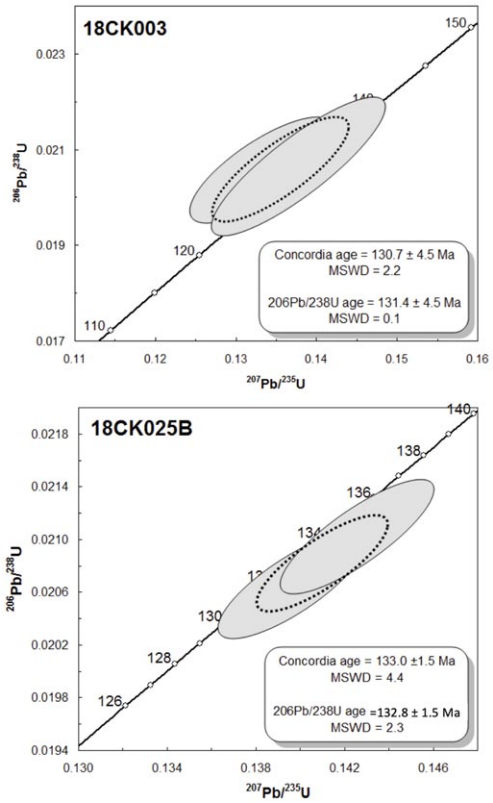

Figure 4. *U-Pb concordia diagram of (**A**) Sample 18CK003 from the northern Knersvlake subswarm and (**B**) Sample 18CK025B from the Doring-Tanqua subswarm, both from the Cederberg Dyke Swarm (CDS). Dashed ellipses define the concordia age.*

Ar-Ar geochronology

Four samples were collected from the CDS and three samples from the east-west dykes for a total of seven samples. The four Cederberg samples with new Ar-Ar age determinations include the

two Cederberg samples from which we report U-Pb baddeleyite ages. Cederberg dyke sample 18CK004 was collected on the side of the R355 road from a 75 m wide dyke that strikes ~315° (32.287°S, 19.662°E). Cederberg sample 18CK006 was collected from a ~25 m wide, 320° striking dyke adjacent to a road within Tanqua National Park (32.450°S, 19.962°E).

Two of the east-west dykes were collected along the Atlantic coast, with sample 19CK001 being collected 27 km southeast of Kleinsee from a 10 m wide dyke and sample 19CK006 collected from a 10 m wide dyke 163 km southeast Kleinsee. The third east-west dyke sample (19CK003) was collected inland from a 20 m wide dyke situated within a farm ~7 km east of the N7 highway and 3 to 4 km north of the provincial boundary separating Northern and Western Cape.

The Ar isotope data are listed in Appendix Table 2 and age spectra as well as inverse isochron diagrams are shown in Figure 5. The Ca/K ratios of included steps as derived from $^{37}Ar/^{39}Ar$ ratios are low, mostly between 1 and 5, signaling high K contents for basalts (see Appendix Tables 2 and 3). Cl/K ratios (from $^{38}Ar/^{39}Ar$) are below 0.01, indicative of low degrees of alteration.

The samples contain significant amounts of ^{36}Ar. In all cases except 19CK001A, inverse isochron regressions of the included step results yielded Y-axis intercepts showing initial $^{40}Ar/^{36}Ar$ ratios overlapping, within uncertainty limits, the atmospheric value of 298.56 ± 0.31 (Lee et al., 2006). The results shown in these age spectra were therefore corrected using this atmospheric $^{40}Ar/^{36}Ar$ ratio. For 19CK001A, the regressions of included steps for both duplicates yielded initial $^{40}Ar/^{36}Ar$ ratios of *ca.* 400 (although with a very large error for 19CK001A-1). These values (and their uncertainties) were used to calculate the age spectra. This resulted in a *ca.* 6 Ma younger age for 19CK001A-2 than if atmospheric argon were used, whereas the age for 19CK001A-1 remained unchanged, and thus both duplicates yield identical spectrum ages, well within analytical uncertainties.

The fraction of ^{39}Ar included steps that range from 60 to 93% with only one sample (18CK006) yielding a visibly disturbed spectrum. To assess the validity of the spectra, we use the mean square of weighted deviations (MSWD) for the included steps, and its critical value

$$MSWD = \frac{1}{n-1}\sum_{i=1}^{n}\frac{(x_i - x_{av})^2}{\sigma_i^2}$$

and

$$MSWD_{crit} = 1 + 2\sqrt{\frac{2}{(n-1)}}$$

where n is the number of included steps, *av* stands for average and σ_i is the uncertainty of step i. If MSWD > $MSWD_{crit}$ then there is a 95% probability that factors other than the analytical error are contributing to the uncertainty (Schaen et al., 2021). Clearly, small analytical errors increase the MSWD value, as seen in sample 19CK003 (Figure 5) which present near-plateaus while having MSWD≈$MSWD_{crit}$. All other samples have MSWD < $MSWD_{crit}$ and confidence in these results is good.

The $^{40}Ar/^{39}Ar$ ages of the four CDS samples cluster between 128.5 ± 1.4 to 132.1 ± 1.4 Ma. For example, 18CK003 $^{40}Ar/^{39}Ar$ result is identical within error limits to its baddeleyite U-Pb age, whereas for sample 18CK025B its $^{40}Ar/^{39}Ar$ age is, outside errors, 4.3 myr younger than its baddeleyite U-Pb age (Figures 4 and 5); see discussion of age discrepancy in section 4.1. Among the east-west-trending dykes, 19CK001A and 19CK003 have, within uncertainty limits, identical *ca.* 140 Ma ages (Figure 5).

Pooled gas ages (also referred to as integrated ages), are calculated from the argon released in the steps within an indicated range, and both the age and isotopic uncertainties are obtained from this pool. Thus, the error obtained in a pooled age is usually smaller than the standard deviation of the individual step results. The isochron ages and spectrum pooled gas ages are seen to agree within uncertainty, with the latter being more precise. The Cl/K ratios are uniformly low, indicating no significant alteration, except for the lowest-temperature steps.

Geochemistry

The new data we report herein consists of ten samples collected from the CDS, many of which have been used for the age determinations previously described. These ten samples were collected from nine sample sites (18CK025A and B were collected from the same location) and, based on Google Earth® imagery, from seven separate dykes. In addition to the Cederberg dykes, we report the results from two samples collected from east-west dykes that are located to the north of the CDS (Figure 2). Because of a high LOI in sample 19CK006 (LOI 6.88%), we will not use this sample further in this section and that of the discussion for interpretive purposes. As most of these samples also have associated geochronology data, coordinate and sample site data have been described above, in the previous two sections. The geochemical results which also include coordinate data are presented in Appenix Table 3. As shown in Figure 6, the CDS and the two samples from the east-west dykes are basaltic andesite to borderline andesitic based on Total Alkali-Silica (TAS, SiO_2 versus Na_2O+K_2O) systematics from LeBas et al., (1986).

Based on Sun and McDonough (1989) chondrite-normalised, rare-earth element (REE) systematics (Figure 7), the Cederberg and FBDS samples demonstrate similar parallel patterns, having shallow light REE (LREE) enriched slopes, between La and Gd, along with nearly flat heavy REEs (HREEs), between Tb and Lu. Europium (Eu) anomaly is either weakly negative or absent in the studied dykes. The east-west dykes on the other hand, diverge slightly by exhibiting distinctly steeper LREE- slopes together with slightly sloping HREE-patterns.

Expanding the multi-element systematics, Figure 8 shows a primitive-mantle-normalised multi-element plot (normalised to primitive mantle in Sun and McDonough, 1989). The studied dykes (Cederberg, east-west) along with the False Bay Dykes of Backeberg et al. (2011) display positive Pb anomalies along with pronounced negative Nb- Ta and variable Sr anomalies. We note here the presence of a strong negative Nb anomaly despite the use of the tungsten carbide mill as indicated in the methods section. With the exception of Ba, the absence of a large-ion lithophile element (LILE) scatter, in addition to the fresh nature of these samples (see the petrography section), are all indicative of low degrees of alteration and elemental

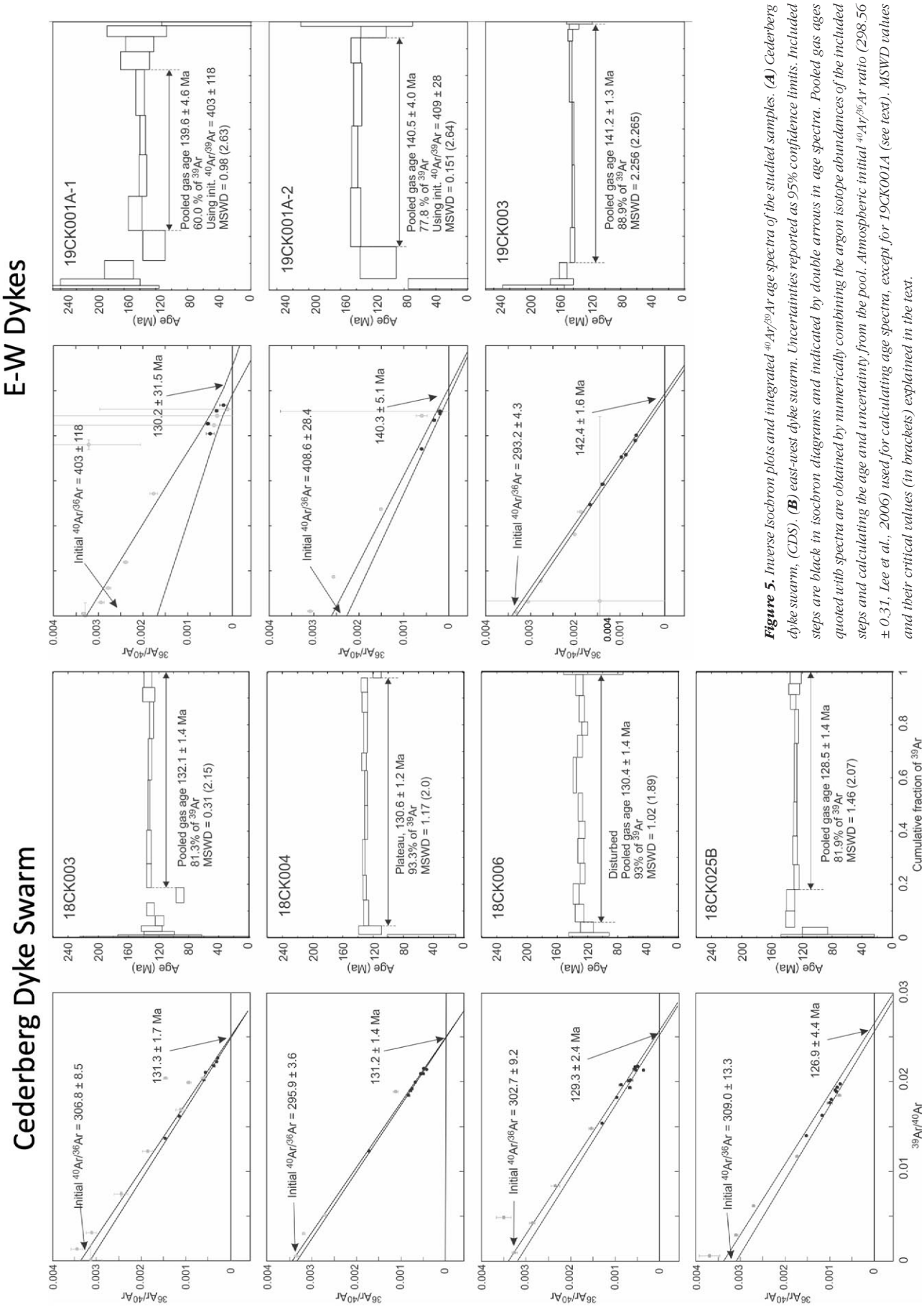

Figure 5. *Inverse isochron plots and integrated $^{40}Ar/^{39}Ar$ age spectra of the studied samples. (**A**) Cederberg dyke swarm, (CDS). (**B**) east-west dyke swarm. Uncertainties reported as 95% confidence limits. Included steps are black in isochron diagrams and indicated by double arrows in age spectra. Pooled gas ages quoted with spectra are obtained by numerically combining the argon isotope abundances of the included steps and calculating the age and uncertainty from the pool. Atmospheric initial $^{40}Ar/^{36}Ar$ ratio (298.56 ± 0.31, Lee et al., 2006) used for calculating age spectra, except for 19CK001A (see text). MSWD values and their critical values (in brackets) explained in the text.*

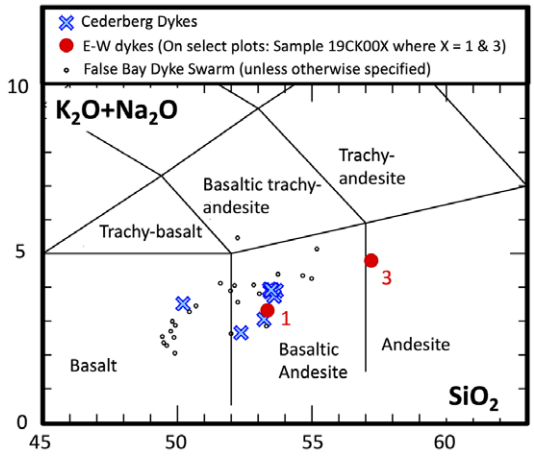

Figure 6. *Total Alkali Silica (TAS) systematics of the Cederberg Dyke Swarm (CDS) along with the east-west dykes (our samples) and that of the False Bay Dyke Swarm (FBDS) (Backeberg et al., 2011). The underlying systematics are from LeBas et al. (1989). The smaller black circles represent legacy data from the FBDS and is significantly smaller than the symbols we report for this study.*

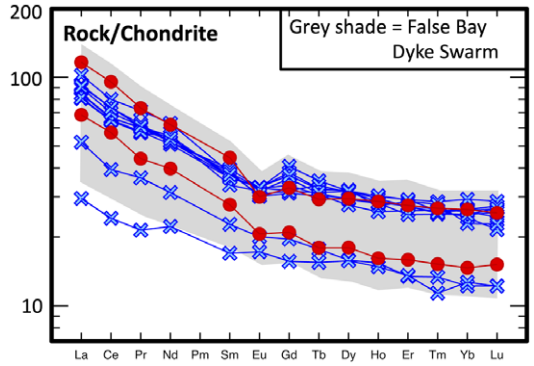

Figure 7. *Chondrite-normalised rare-earth element plot of the Cederberg dykes, the east-west dykes plotted against legacy False Bay dykes data of Backeberg et al. (2011). Normalisation of data is from Sun and McDonough (1989). Symbols as in Figure 6.*

mobility of these samples. Thus, the LILE/HFSE-enrichment in these patterns likely reflects that of their source.

We next plot the CDS and east-west dyke results along with FBDS data from Backeberg et al. (2011) on a MgO versus Th/NbPM diagram (Figure 9A; PM = normalised to primitive mantle values derived from McDonough and Sun (1995)). With regards to the FBDS, a trend of increasing Th/NbPM values as MgO decreases is manifest. Most of our Cederberg dyke results show near uniformly high Th/NbPM with a narrow MgO range at the lower end of the MgO values from the FBDS (around MgO = 4 wt%). Though we caution that there are only two data points for our east-west dykes, therefore not enough to discern a trend, the sample from the east-west dykes that has the highest Th/NbPM values also has the lowest MgO, which is consistent with the FBDS trend.

Plotting Th/NbPM versus La/NbPM (Figure 9B), with the exception of one Cederberg dyke sample 18CK003, all other samples exhibit a well-defined trend from where most oceanic basalts (specifically MORB) plot towards relatively low ratios and up along a trajectory towards an upper, rather than a lower, crust. For Figure 9B, upper crust data is from Rudnick and Fountain (1995) and lower crustal data is from Weaver and Tarney (1984). Our Cederberg dyke data, furthermore, generally plot on top of the FBDS dataset of Backeberg et al. (2011). Both east-west

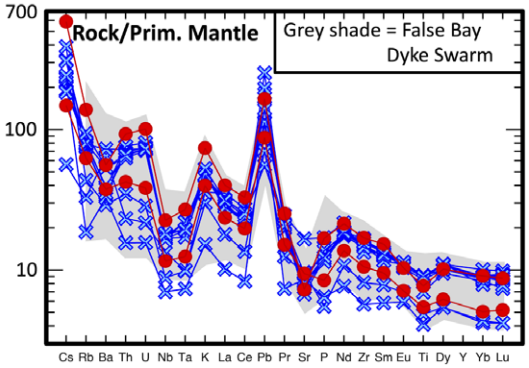

Figure 8. *Primitive mantle normalised trace element diagram of the Cederberg dykes, the east-west dykes plotted against legacy False Bay dykes data of Backeberg et al. (2011). Primitive mantle normalisation is from McDonough and Sun (1995). Symbols as in Figure 6.*

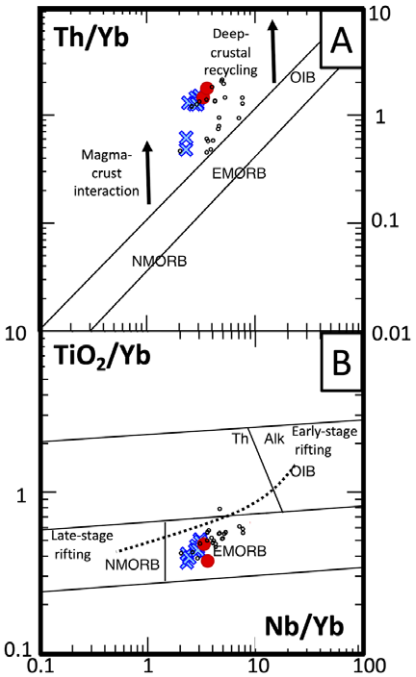

Figure 9. *(**A**) MgO versus Th/Nb$_{PM}$ and (**B**) La/Nb$_{PM}$ versus Th/Nb$_{PM}$ diagrams, with our data and that of the False Bay Dyke Swarm (FBDS) of Backeberg et al. (2011) plotted. Ratios normalised to primitive mantle (PM) values of McDonough and Sun (1995). Upper crust trend from Rudnick and Fountain (1995) and lower crust trend from Weaver and Tarney (1984). Symbols as in Figure 6.*

dykes display elevated Th/Nb_{PM} and plots on top of Cederberg dyke samples that are also elevated in Th/Nb_{PM}.

Our data, when plotted on a Nb/Yb versus. Th/Yb diagram after Pearce (2008) diagram reveal that, relative to true E-MORB basalt, the CDS and two samples from the east-west dykes are variably enriched in Th (Figure 10A). Additionally, when these samples are plotted on a Nb/Yb versus TiO_2/Yb diagram after Pearce (2008; Figure 10B), the basalts and basaltic andesites of the CDS and the east-west dykes appear chemically equivalent to an Enriched Mid-Ocean Ridge Basalt (E-MORB) that we will discuss the nuances of later.

A geochemical plot developed by Pearce et al. (2021) permits fingerprinting of LIP-connected volcanics (e.g., continental flood basalts) and intrusions (dykes and sills) when plotted on TiO_2/Yb versus Th/Nb (Figure 11A to C). Using this plot, the data show that samples from the CDS and the east-west dykes have elevated Th/Nb and plot within the Subduction-Modified Lithospheric Mantle (SZLM array), labeled on this diagram as the

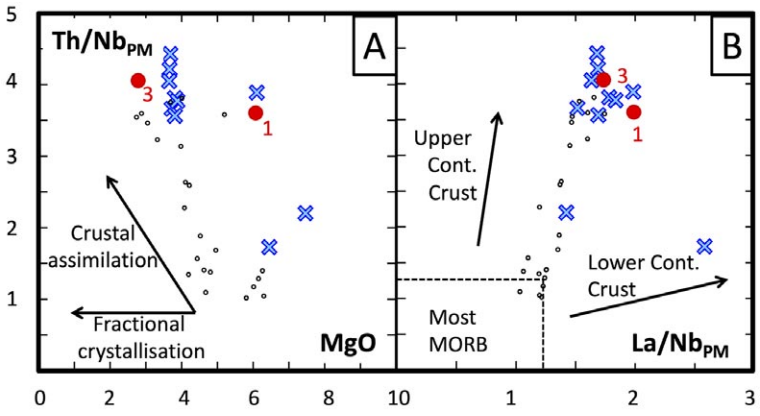

Figure 10. *(**A**) Nb/Yb versus Th/Nb and (**B**) Nb/Yb versus TiO_2/Yb plot showing our dyke data as well as the False Bay dykes from Backeberg et al. (2011). Underlying systematics are from Pearce (2008). Key to field names: EMORB=Enriched Mid Ocean Ridge Basalt; NMORB=Normal mid-ocean ridge basalt; OIB=Ocean Island Basalt; Th (in plot)=tholeiitic and Alk=alkaline. Symbols as in Figure 6.*

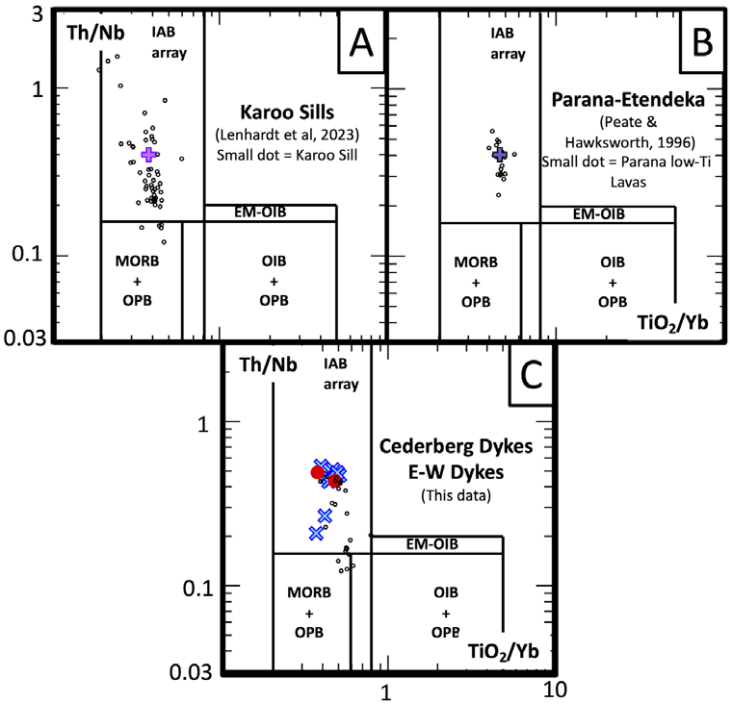

Figure 11. *TiO_2/Yb versus Th/Nb systematics of Pearce et al. (2021). (**A**) Data of Karoo Sills from Lenhardt et al (2023); (**B**) Data of Low-Ti lavas from the Paraná-Etendeka LIP (Peate and Hawksworth, 1996); (**C**) Our data along that of the False Bay Dyke Swarm (FBDS) (Backeberg et al., 2011). Key to geochemical field abbreviations in C: K=Karoo Sills (as in (A)) and P-E=Paraná-Etendeka (as in (B)). The large crosses in (A) and (B) represent the average composition of Karoo sills and Paraná-Etendeka low-Ti lavas, respectively.*

"IAB (CC) Array" (IAB=Island Arc Basalts; CC=Continental Crust) that is above the plume array (Figure 11C). We note here that Pearce and others (2021) also indicate that elevated Th/Nb represents a proxy for crustal assimilation. Most of the data from the Backeberg et al. (2011) FBDS dataset also plot within the IAB (CC) array, but a few low Th/Nb samples occupy the MORB + Ocean Plate Basalt (OPB) field of the Plume array.

Discussion

General synopsis

Our six U-Pb and $^{40}Ar/^{39}Ar$ ages for the Cederberg dykes and two $^{40}Ar/^{39}Ar$ determinations for east-west dykes (Figures 4 and 5) preclude any correlation with the *ca.* 182 Ma Karoo LIP, despite its regional proximity (e.g., Svensen et al., 2012). Instead, these age results confirm a temporal association with the southern proto-Atlantic rifting and breakup (Lovecchio et al., 2020; White and McKenzie, 1989). We note the greater range of the Ar-Ar ages (132 to 128 Ma, 132.1 ± 1.4 Ma, 130.6 ± 1.2 Ma, 130.4 ± 1.4 Ma and 128.5 ± 1.4 Ma) in comparison with the U-Pb ages (133.0 ± 1.5 Ma and 131.4 ± 4.5 Ma), and the difference in U-Pb and Ar-Ar ages for the same sample (18CK028B), 128 Ma Ar-Ar and 133 Ma U-Pb age. We begin by exploring the magmatic source(s) and evolution of the Cederberg and east-west dykes with particular attention towards discussing whether a mantle plume might be involved in addition to magmatic processes associated with rifting and crustal contamination or other mantle source(s).

As shown in Figure 1, the CDS is roughly parallel to the FBDS (Backeberg et al., 2011), located ~50 km farther south. The multi-element plots in Figures 7 and 8 show a remarkable overlap between the Cederberg and FBDS, with similar weakly enriched LREE slopes in tandem with a near flat HREE slope, a resemblance that is further accentuated by both additional high field strength and large ion lithophile elements (HFSE and LILE, respectively). Based on their matching geochemistry, geochronology (~130 Ma) and parallel trends the CDS can be considered a peripheral extension of the False Bay dykes and, thus can be combined into a single swarm, herein referred to the GCFDS.

The east-west dykes are a few million years older than the GCFDS and do not overlap within the 2σ error margin age of 140 Ma and have slightly different REE and unrelated HFSE and LILE patterns (Figures 7 to 8) with respect to the Cederberg and False Bay dykes. Therefore, the presence of the east-west dykes could be recording a precursory phase of magmatism related to initial rifting processes within a nascent rifted margin just prior to the first formation of oceanic crust. Work by Moulin et al. (2010) place the first appearance of oceanic crust in the Southern Atlantic at 130 to 134 Ma. However, with only two samples from the east-west dykes, it is difficult to make other observations that would lead to robust petrogenetic interpretations.

Role(s) of subduction-modified lithospheric mantle and/or crust

One way to explain the geochemical signatures of the GCFDS is through the crustal contamination of an asthenospheric mantle-derived magma. Figure 9B indicate that most data conform to the assimilation of an upper continental crust, which would then require an upper crustal magma chamber for all dykes. Further support for the continental crust being involved, is supported by Figure 9A (MgO versus Th/Nb_{PM}) plot, which shows that a decrease in MgO is moderately associated with a concomitant increase in $(Th/Nb)_{PM}$ and could additionally indicate an Assimilation-Fractional Crystallisation (AFC) process. That being said, two Cederberg dyke samples returned elevated Th/Nb_{PM} values, when compared with FBDS-samples with similar high MgO. This could indicate the existence of two magma suites that each underwent crustal contamination processes independently. As a common alternative, similar geochemical signatures can also be induced through interaction with a metasomatised lithospheric mantle in subduction-related processes (e.g. Pearce et al., 2021) or through rift-related processes (e.g. 713 Ma Tatonduk dykes; Cox et al., 2018).

The LIP-Printing discrimination diagrams by Pearce et al. (2021) indicate that the Cederberg – FBDS, along with the east-west dykes, have incompatible element ratio characteristics that indicate input of crustal components (either from direct interaction with crustal rocks or from interaction with subduction-modified metasomatised lithospheric mantle; Figure 11C). This data overlaps with where most low-Ti basalts of the world plot in Figure 14A of Pearce et al., (2021). More succinctly, our CDS data and data from two east-west dykes plot within the IAB (CC) field (Pearce et al. 2021), who also considers the SZLM a proxy for crustal involvement. Additionally, the FBDS of Backeberg et al. (2011) plot between a transitional MORB-like mantle source and the IAB (CC) Array. According to Pearce et al. (2021), such a transitional MORB-like asthenospheric mantle only needs to incorporate small quantities of SZLM (or similar continental crust) to push their incompatible element ratios well into the IAB (CC) Array (with higher Th/Nb). In contrast, more "enriched" plumes (OIB) or low-degree melts of "normal" plume magmas (towards higher TiO_2/Yb) generally need to incorporate significantly more SZLM or continental crust to push their incompatible element ratios into the IAB (CC) Array. The CDS data, extending from an enriched MORB mantle source region up into the IAB (CC) Array of Figure 11C, strongly suggest that these magmas melted from a mantle source intermediate between depleted and enriched mantle (E-MORB-like) that subsequently incorporated upper continental crust upon its ascent.

Using LIP-Printing plot by Pearce et al. (2021), (Figure 11), the dispersions for the CDS, east-west dykes and the FBDS are compared with the dispersions and arithmetic mean of nearby Karoo low-Ti Sills (Figure 11A; Lenhardt et al., 2023) and coeval Etendeka Low-Ti lavas (Figure 11B; Peate and Hawksworth, 1996) and result in several observations. The first observation is that the average compositions of all three provinces are essentially indistinguishable from our CDS, east-west dykes and the most Th/Nb-elevated FBDS dykes (Figure 11A to C). We further observe that Karoo sills vary the most in Th/Nb, plotting essentially throughout the range of the IAB array, which – as previously indicated – is likely a proxy for continental crust involvement. However, some low-Th/Nb Karoo data also plot within the low-TiO_2/Yb MORB field of this diagram's mantle

array. Conversely, the dispersion of the Etendeka low-Ti lavas is more restricted, plotting entirely within this IAB-array. It is thus, notable how similar the CDS, east-west dykes and the FBDS which we now will call the Greater Cederberg-False Bay Large Igneous Province (GCF-LIP), resemble both *ca.* 50 myr older Karoo sills and coeval low-Ti Paraná lavas that erupted ~1 500 km north of these from a LIP-printing perspective.

Potential role of mantle plumes

The issue of whether or not plumes are involved in LIPs that are overprinted by geochemical signatures from either continental crust or SZLM is a point of intense debate (e.g. Sections 4.2 and 5.2 of Pearce et al., 2021 and references therein). In consideration of the data presented herein, we suggest that mafic magmatism, which fed Cederberg Dykes, east-west dykes along with the FBDS, resulted primarily from initial melting within an upper mantle source (flat HREE pattern, Figure 7). The initial composition of this source is consistent with producing an E-MORB-like basaltic magma (Figure 10) the melting of which was fueled in part by decompression melting below a proto-Atlantic rift. Pearce (2008) demonstrates that, in the context of rift-related magmatism, basaltic samples which plot in the upper OIB array on a Nb/Yb versus TiO_2/Yb diagram (our Figure 10B), serve as proxy for melting during early stages of rifting when the crust is thick enough to restrict initial melting from garnet peridotites. In contrast, Pearce (2008) show that basaltic samples plotting in the lower MORB array of the same diagram (Figure 10B) reflects magmatism during later stages of rifting when the crust is thinner. In particular, the fact that our data plots in the lower MORB array of Figure 10B, rather than the upper OIB array suggest substantial crustal thinning already took place. Such primary magmas then assimilated upper crustal material (Figure 9A and B). It is possible then, that at some point of magma evolution, the thermal pulse from a mantle plume could have assisted in creating the conditions favorable towards melt production in an extensional tectonic regime, even though the geochemical evidence for mantle plume involvement is not robust.

Even if the geochemical data cannot conclusively verify the involvement of an enriched mantle plume, other observations do. The first indication stems from the apparent converging trends shown by the CDS, east-west Dykes and the FBDS to a now offshore magmatic center. However, such a center must have been active for ~10 myrs in order to supply magmas for the earliest east-west dykes and younger dyke swarms (Figure 12). Secondly, there appears to be a clustering of magmatism at three nodes along the southern Atlantic, as indicated in Figure 12A. These three nodes include the well-known Paraná-Etendeka LIP that was initiated by the Tristan mantle plume (Duncan, 1981; White and McKenzie, 1989; O'Connor and Duncan, 1990; O'Connor et al., 2012), an intermediate BOR-LIP to the north associated with the St. Helena plume (Matos, 2021) and a southern node which we will call the GCF-LIP. A review of dyke thicknesses in different setting shows that average dyke widths of >10 m are not generally associated with magmatic processes found in subduction zones, spreading ridges or individual central volcanoes and instead are a characteristic of plume-related LIPs (Ernst et al., 1995; Ernst, 2014 and references therein). We note that field measurements of Cederberg dykes returned widths that range from 10 m to 90 m, providing field evidence of potential plume involvement. Finally, several minor aseismic ridges extend from the southern west coast of Africa, which have previously been interpreted as hot spot tracks. One of these tracks, the Discovery seamount track, at 135 Ma, occupied a region just off the northern South Africa Coast where dykes associated with the GCF-LIP show convergence (Figure 12B). Thus, we suggest, that there may well have been a minor mantle plume (or ridge) initiator to the GCF-LIP, which must have been hotter than its surrounding upper mantle but not necessarily as enriched, or its geochemical signatures were masked by the lithospheric overprint as proposed above.

One could theoretically ascribe the northern component of the GCFDS to be part of a circumferential system encircling the proto-Tristan plume centre (e.g. Buchan and Ernst, 2019). However, this is inconsistent with the concave south curvature of at least the Cederberg dykes, while the two coastal east-west dykes could still be part of such a circumferential swarm.

It has been established that the Atlantic Ocean rifting sequence was facilitated by three main plume centres: the 200 Ma plume centre associated with the Central Atlantic Magmatic Province (CAMP), the *ca.* 135 Ma Tristan plume centre associated with the Paraná-Etendeka LIP and finally the proto-Icelandic plume that gave rise to the 55 to 60 Ma North Atlantic Igneous Province (White and McKenzie, 1989; Ernst, 2014 and references therein). While these three plume centres represent "major players" in the rifting sequence, smaller intraplate mantle plumes may also have played a role. Indeed, while the Paraná-Etendeka LIP represents a major magmatic event at 135 Ma, a recently identified 135 Ma Equatorial Atlantic Magmatic Province (EQUAMP) in northeast Brazil by Hollanda et al. (2019), can be linked to a proto-St. Helena plume. Further research reveals this node of magmatism, now referred as the BOR-LIP, to be even larger than previously thought (Matos, 2021). If true, then at least two separate LIPs of approximately the same age have been identified as having been proximal to each other (their plume centres separated by about 2 500 km). This leads to the question whether the up to 90 m thick Cederberg, False Bay and east-west dykes in South Africa, which do not trend towards the paleo-Tristan plume centre, had their own, more localised, plume source? Work by O'Connor et al. (2012) in the South Atlantic identified five distinct hotspots trails from hotspots that originally arose from the margins of the Africa large low seismic velocity province (LLSVP). These hotspot trails from north to south are Tristan, Gough, Discovery, Shona and Bouvet. In their Figure 3 (and modified by our Figure 12B), O'Connor et al. (2012) show that the Tristan and Gough tracks parallel with the Walvis Guyots and Walvis Ridge and both tracks (Tristan and Gough) intersect with the continental slope offshore of northern Namibia. On the other hand, O'Connor et al. (2012) showed that the Discovery hotspot, when reconstructed back to 135 Ma, appears to have occupied what is now the border region between the northern South African Atlantic coast and the extreme southern Namibian coast. The coast-perpendicular, *ca.* 140 Ma dykes along with the coast-oblique Cederberg and False

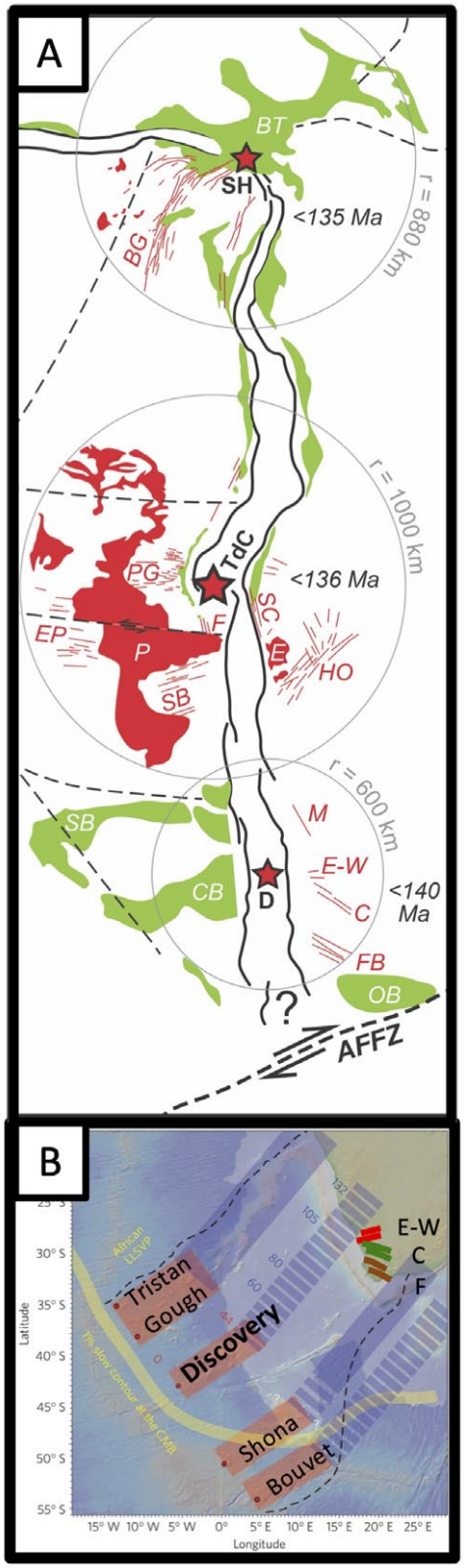

Bay dykes appear to form a quasi-radiating pattern with a possible focus in the region where O'Connor et al. (2012) predicted the Discovery plume and hot spot at *ca*. 135 Ma (Figure 12B) occupied.

The Discovery plume appears to have occupied a region either proximal to or at the centre of a triple-junction where two arms represent incipient Atlantic rifting and the Salado Rift Basin representing a third aulacogen arm (Figure 12A). It should be noted however, that the incipient rifting at *ca*. 130 Ma, which ultimately resulted in the Atlantic Ocean, also reactivated rifting in the Salado Basin, as initial rifting had occurred during the *ca*. 183 Ma Karoo LIP event, supposedly as a far-field tectonic effect (Lovecchio et al., 2020).

When observed together, the 135 Ma EQUAMP with a potential St. Helena plume source, the 135 Ma Paraná-Etendeka LIP with a likely Tristan plume source, and the 135 Ma magmatic province, we herein propose to call the GCF-LIP, which potentially arose from the Discovery plume, appear to have originated from a ~3 300 km long mantle plume "curtain" at the edge of the Africa Large Low Seismic Velocity Province (LLSVP; Figure 12B). The coeval Paraná-Etendeka and GCF-LIP were probably fed from two different plume sources rather than one, which would help to explain the complex orientations and patterns of *ca*. 135 Ma dykes in the southern African Atlantic coast and formerly adjacent South America, especially with dykes in South Africa (Figure 12A; Demarco et al., 2020). Finally, with a Discovery plume source for the GCF-LIP, it is possible to consider that the 140 to 120 Ma kimberlite fields of South Africa, which Ernst and Jowitt (2013) mention as a potential magmatic product of the Paraná-Etendeka LIP, may in fact be genetically related to the GCF-LIP rather than the Paraná-Etendeka plume centre. Ernst and Jowitt (2013) have demonstrated that many large-scale kimberlite events are spatially and temporally associated with LIPs and may be generated in portions of mantle plumes that are located beneath cratons which are too thick for normal basaltic melting. Ernst et al. (2018) highlight, in particular, the strong link between two LIP events in Siberia: the 370 Ma Yakutsk-

Figure 12. *(**A**) Compilation map of 130 to 140 Ma magmatism associated with South Atlantic rifting as modified from the 134 Ma tectonic reconstruction from Moulin et al. (2010). Red stars represent hotspots, red lines indicate dykes, red polygons represent volcanic rocks, green polygons represent syn-breakup basins. Key to abbreviations: For hotspots: D=Discovery; SH=St. Helena; TdC=Tristan da Cunha; for volcanics: E=Etendeka; P=Paraná; for dyke swarms: BG=Borborema Giant dyke swarm; C=Cederberg dyke swarm (CDS) (this paper); east-west=east-west dykes (this paper); EP=Eastern Paraguay Dyke Swarm; F=Florianopilis Dyke Swarm; FB=False Baydyke swarm; HO=Henjes Bay-Outjo dyke swarm; M=Mehlberg dyke swarm; PG=Ponta de Grossa dyke swarm; SB=South Brazil dyke swarm; SC=Skeleton Coast dyke swarm; for basins: BT=Benue Trough; CB=Colorado Basin; SB=Saladao River Basin; OB=Outeniqua Basin; for fault zone: AFFZ=Agulhas-Falkland Fault Zone. Sources of information used for this compilation are Moulin et al. (2010), O'Connor et al. (2012), Hollanda et al. (2019), Demarco et al. (2020) and Matos (2021). (**B**) Hot spots and their tracks of the south Atlantic along with their seamounts and ridges interpreted to be hot spot trails. FBDS (F), Cederberg dyke swarm (CDS) (C) and east-west dykes (E-W) have been added showing a proto-fanning pattern with a focus coincident with a possible proto-Discovery hotspot origin. Modified from O'Connor et al. (2012).*

Vilyui LIP and 375 to 345 Ma kimberlites along with the 245 to 215 Ma kimberlites associated with the 252 Ma Siberian Traps (Table 6 in Ernst and Jowitt, 2013 provide additional examples along with associated references).

Conclusions

This study provides new age and geochemical data for the CDS in addition to two east-west dykes north of the CDS. We make four key findings:

- Two U-Pb age determinations along with four $^{40}Ar/^{39}Ar$ ages confirm that the Cederberg dykes intruded at 130 to 133 Ma. Two Ar-Ar age determinations of east-west dykes north of the CDS give *ca.* 140 Ma ages. These results preclude that these dykes belong to the *ca.* 180 Ma Karoo LIP event.
- The Cederberg dykes along with the FBDS and east-west dykes are composed of an Enriched Mid-Ocean Ridge Basalt (E-MORB) mantle array component that is transitional between N-MORB and OIB. This transitional magma later assimilated upper continental crustal components,.
- The geochemical similarities between the Cederberg and False Bay dykes along with their parallel trends and matching ages suggest that the Cederberg dykes are a northern extension of the FBDS and thus can be collectively known as the Greater Cederberg-False Bay Dyke Swarm (GCFDS).
- The Greater FBDS and the east-west dykes to its north strongly suggest magmatism during a time of active rifting, defining a partial radiating pattern with a focal point just offshore of the borderlands between South Africa and Namibia. The evidence presented here, including field evidence (dyke widths up to 90 m), supports mantle melting was mostly facilitated by rift-related decompression melting process but with a strong likelihood that this melting was additionally facilitated by the upwelling of a minor mantle plume. We propose that the proto-Discovery mantle plume influenced the formation of these dykes during a period of active rifting. We hence establish a Greater Cederberg False Bay Large Igneous Province (GCF-LIP) separate from the Paraná-Etendeka LIP with its Tristan plume source 1 300 km to the north.
- Three *ca.* 130 Ma LIPs/plume centres are now recognised along the South Atlantic margins (from south to north): GCF-LIP (Discovery plume), Paraná-Etendeka LIP (Tristan plume) and BOR-LIP (St. Helena plume). The presence of these three 130 Ma centres spaced over a distance of greater than 2 000 km can be inferred to be collectively linked to the opening of the South Atlantic.

Acknowledgements

C.G. Kingsbury and W. Altermann are indebted to the South African DSI-NRF Centre of Excellence for Integrated Mineral and Energy Resource Analysis (DST-NRF CIMERA) for funding. J.D. Kramers thanks the South African National Research Foundation (NRF) for grants 81022 and 115260. Opinions expressed and the scientific conclusions heretofore rendered are those of the author(s) and are not necessarily attributed to DSI-NRF-CIMERA or NRF. R.E. Ernst has been partially supported by the Russian Science Foundation (grant No. 18-484 17-00240) and along with C.G. Kingsbury is supported through a MegaGrant Award through the Russian Federation. We are indebted to T. Makhubela for his insights and assistance during the revisions process. Additionally, this contribution benefited through the thoughtful comments from S. Denyszyn and an anonymous reviewer which helped improve this manuscript. Finally, we thank the Editor, M.A. Elburg for editorial handling. This is Publication No. 92 of the LIPs- Industry Consortium project (www.supercontinent.org) and was partially funded by the Consortium with matching funds from Canadian NSERC grant No. CRD CRDPJ 523131-17.

References

Almeida, V. V, Janasi, V.A., Heaman, L.M., Shaulis, B.J., Hollanda, M.H. and Renne, P.R., 2018. Contemporaneous alkaline and tholeiitic magmatism in the Ponta Grossa Arch, Paraná-Etendeka Magmatic Province: Constraints from U-Pb zircon/baddeleyite and $^{40}Ar/^{39}Ar$ phlogopite dating of the José Fernandes Gabbro and mafic dykes. Journal of Volcanology and Geothermal Research, 355, 55-65. doi:10.1016/j.jvolgeores.2017.01.018

Backeberg, N.R., Reid, D.L., Trumbull, R.B. and Romer, R.L., 2011. Petrogenesis of the FBDS, Cape Peninsula, South Africa: evidence for basement assimilation. South African Journal of Geology, 114, 335-352. doi:10.2113/gssajg.114.3-4.335

Baksi, A.K., Archibald, D. and Farrar, E. 1996. Intercalibration of $^{40}Ar/^{39}Ar$ dating standards. Chemical Geology, 129, 307-324.

Buchan, K.L. and Ernst, R.E., 2019. Giant circumferential dyke swarms: Catalogue and Characteristics. In: R. Srivastava, R.E. Ernst and P. Peng (Editors), Dyke Swarms of the World: A Modern Perspective. Springer Geology, Singapore, 1-44. doi:10.1007/978-981-13-1666-1_1

Council for Geoscience, 2019. Geological map of the Republic of South Africa and the Kingdoms of Lesotho and Swaziland. Council for Geoscience, scale 1:1,000,000.

Cox, G.M., Halverson, G.P., Denyszyn, S., Foden, J. and Macdonald, F.A., 2018. Cryogenian magmatism along the north-western margin of Laurentia: Plume or rift? Precambrian Research, 319, 144-157.

Demarco, P.N., Masquelin, H., Prezzi, C., Aïfa, T., Muzio, R., Loureiro, J., Peel, E., Campal, N. and Bettucci, L.S., 2020. Aeromagnetic patterns in Southern Uruguay: Precambrian-Mesozoic dyke swarms and Mesozoic rifting structural and tectonic evolution. Tectonophysics, 789, 228373. doi:10.1016/j.tecto.2020.228373

Duncan, R.A., 1981. Hotspots in the southern oceans - an absolute frame of reference for motion of the Gondwana continents. Tectonophysics, 74, 29-42.

Ernst, R.E., 2014. Large Igneous Provinces. Cambridge University Press, Cambridge, UK. 514p

Ernst, R.E., Davies, D.R., Jowitt, S.M. and Campbell, I.H., 2018. When do mantle plumes destroy diamonds? Earth and Planetary Science Letters, 502, 244-252.

Ernst, R.E., Head, J.W., Parfitt, E., Grosfils, E. and Wilson, L., 1995. Giant radiating dyke swarms on Earth and Venus. Earth Science Reviews, 39, 1-58.

Ernst, R.E. and Jowitt, S.M., 2013. Large Igneous Provinces (LIPs) and Metallogeny, In: Tectonics, Metalogeney, and Discovery: The North American Cordillera and Similar Accretionary Settings. Society of Economic Geologists Special Publication, 17, 17-51.

Florisbal, L.M., Heaman, L.M., Janasi, V.A. and Bitencourt, M.F., 2014. Tectonic significance of the Florianópolis Dyke Swarm, Paraná- Etendeka Magmatic Province: A reappraisal based on precise U-Pb dating. Journal of Volcanology and Geothermal Research, 289, 140-150. doi:10.1016/j.jvolgeores.2014.11.007

Gomes, A.S. and Vasconcelos, P.M., 2021. Geochronology of the Paraná-Etendeka large igneous province. Earth-Science Reviews, 220, 103716.

Hollanda, M.H.B.M., Archanjo, C.J., Macedo Filho, A.A., Fossen, H., Ernst, R.E., de Castro, D.L., Melo, A.C. and Oliveira, A.L., 2019. The Mesozoic equatorial

Atlantic magmatic province (EQUAMP): A new large igneous province in South America. In: R. K. Srivastava (Editor), Dyke Swarms of the World: A Modern Perspective. Springer Nature, 87-110. doi:10.1007/978-981-13-1666-1_3

Janasi, V.A., Freitas, V.A. and Heaman, L.H., 2011. The onset of flood basalt volcanism, Northern Paraná Basin, Brazil: A precise U-Pb baddeleyite/zircon age for a Chapecó-type dacite. Earth & Planetary Science Letters, 302, 147-153. doi:10.1016/j.epsl.2010.12.005

Jiang, Q., Jourdan, F., Olierook, H.K.H. and Merle, R.E., 2023. An appraisal of the ages of Phanerozoic large igneous provinces. Earth-Science Reviews, 237, 104314. doi: 10.1016/j.earscirev.2023.104314

Kingsbury, C.G., Klausen, M.B., Söderlund, U., Altermann, W. and Ernst, R.E., 2021. Identification of a new 485 Ma post-orogenic mafic dyke swarm east of the Pan-African Saldania-Gariep Belt of South Africa. Precambrian Research, 354, 106043. doi:10.1016/j.precamres.2020.106043

Kossert, K. and Günther, E., 2004. LSC measurements of the half-life of ^{40}K. Applied Radiation and Isotopes, 60, 495-464.

LeBas, M.J., LeMaitre, R.W., Streckeisen, A. and Zanettin, B., 1986. A Chemical Classification of Volcanic Rocks Based on the Total Alkali-Silica Diagram. Journal of Petrology, 27, 745-750.

Lee, J.-Y., Marti, K., Severinghaus, J.P., Kawamura, K., Yoo, H.-S., Lee, J.-B. and Kim, J.-S., 2006. A redetermination of the isotopic abundances of atmospheric Ar. Geochimica et Cosmochimica Acta, 70, 4507-4512.

Lenhardt, N., Galerne, C., Le Roux, P., Götz, A.E. and Lötter, F.J.P., 2023. Geochemistry of dolerite intrusions of the southeastern Main Karoo Basin, South Africa: Magma evolution, evidence for thermogenic gas sequestration, and potential implications for the early Toarcian Oceanic Anoxic Event. Gondwana Research, 113, 144-162.

Lovecchio, J.P., Rohais, S., Joseph, P., Bolatti, N.D. and Ramos, V.A., 2020. Earth-Science Reviews Mesozoic rifting evolution of SW Gondwana: A poly-phased, subduction- related, extensional history responsible for basin formation along the Argentinean Atlantic margin. Earth-Science Reviews, 203, 103138. doi:10.1016/j.earscirev.2020.103138

Ludwig, K.R., 2003. User's manual for Isoplot 3.00: A geochronological toolkit for Microsoft Excel. Berkeley Geochronology Center, Special Publication No. 4, 71.

Matos, R.M.D. de, 2021. Magmatism and hotspot trails during and after continental break-up in the South Atlantic. Marine and Petroleum Geology, 129, 105077. doi:10.1016/j.marpetgeo.2021.105077

Makhubela, T.V., Kramers, J.D., Belyanin, G.A., Dirks, P.H.G.M. and Roberts, E.M., 2017. Proterozoic ^{40}Ar/^{39}Ar ages from cave deposits of the malapa, Sterkfontein and Dinaledi fossil sites, Cradle of Humankind, South Africa. South African Journal of Geology, 120, 21-44.

McDonough, W.F. and Sun, S. -s., 1995. The Composition of the Earth. Chemical Geology, 120, 223-253.

Moulin, M., Aslanian, D. and Unternehr, P., 2010. A new starting point for the South and Equatorial Atlantic Ocean. Earth-Science Reviews, 98, 1-37.

O'Connor, J.A. and Duncan, R.A., 1990. Evolution of the Walvis Ridge-Rio Grande Rise Hot Spot System: Implications for African and South American Plate motions over plumes. Journal of Geophysical Research, 95, 17475-17502.

O'Connor, J.M., Jokat, W., Le Roex, A.P., Class, C., Wijbrans, J.R., Keßling, S., Kuiper, K.F. and Nebel, O., 2012. Hotspot trails in the South Atlantic controlled by plume and plate tectonic processes. Nature Geoscience, 5, 735-738. doi:10.1038/ngeo1583

Pearce, J.A., 2008. Geochemical fingerprinting of oceanic basalts with applications to ophiolite classification and the search for Archean oceanic crust. Lithos, 100, 14-48. doi:10.1016/j.lithos.2007.06.016

Pearce, J.A., Ernst, R.E., Peate, D.W. and Rogers, C., 2021. LIP printing: Use of immobile element proxies to characterize Large Igneous Provinces in the geologic record. Lithos, 392-393, 106068. doi:10.1016/j.lithos.2021.106068

Peate, D.W., 1997. The Paraná-Etendeka Province. In: J.J. Mahony and M.F. Coffin (Editors) Large Igneous Provinces. Washington, DC, American Geophysical Union, 217-245.

Pessano, P.C., Ganade, C.E., Tupinambá, M. and Teixeira, W., 2021. Updated map of the mafic dike swarms of Brazil based on airborne geophysical data. Journal of South American Earth Sciences, 107, 103076.

Pinto, V.M., Hartmann, L.A., Santos, J.O.S., McNaughton, N.J. and Wildner, W., 2011. Zircon U-Pb geochronology from the Paraná bimodal volcanic province support a brief eruptive cycle at ~135 Ma. Chemical Geology, 281, 93-102. doi:10.1016/j.chemgeo.2010.11.031

Ransome, I.G.D., 1992. The geochemistry, kinematics and geodynamics of the Gannakouriep Dyke Swarm. Unpublished M.Sc. thesis, University of Stellenbosch, Stellenbosch, South Africa, 182pp

Reid, D.L., Erlank, A.J. and Rex, D.C., 1991. Age and correlation of the False Bay dolerite dyke swarm, south-western Cape, Cape Province. South African Journal of Geology, 94, 155-158.

Reid, D.L. and Rex, D.C., 1994. Cretaceous dykes associated with the opening of the South Atlantic: the Mehlberg dyke, northern Richtersveld. South African Journal of Geology, 97, 135-145.

Renne, P.R. and Norman, E.B., 2001. Determination of the half-life of ^{37}Ar by mass spectrometry. Physical Review C, 63, 047302.

Renne, P.R., Swisher, C.C., Deino, A.L., Karner, D.B., Owens, T. and DePaulo, D.J., 1998. Intercalibration of standards, absolute ages and uncertainties in ^{40}Ar/^{39}Ar dating. Chemical Geology, 145, 117-152.

Rioux, M., Bowring, S., Dudás, F. and Hanson, R., 2010. Characterizing the U-Pb systematics of baddeleyite through chemical abrasion: application of multi-step digestion methods to baddeleyite geochronology. Contributions to Mineralogy and Petrology, 160, 777-801.

Rudnick, R.L. and Fountain, D.M., 1995. Nature and composition of the continental crust: A lower crustal perspective. Reviews of Geophysics, 33, 267-309.

Schaen, A.J., Jicha, B.R., Hodges, K.V., Vermeesch, P., Stelten, M.E., Mercer, C.M., Phillips, D., Rivera, T.A., Jourdan, F., Matchan, E.L., Hemming, S.R., Morgan, L.E., Kelley, S.P., Cassata, W.S., Heizler, M.T., Vasconcelos, P.M., Benowitz, J.A., Koppers, A.A.P., Mark, D.F., Niespolo, E.M., Sprain, C.J., Hames, W.E., Kuiper, K.F., Turrin, B.D., Renne, P.R., Ross, J., Nomade, S., Guillou, H., Webb, L.E., Cohen, B.A., Calvert, A.T., Joyce, N., Ganerød, M., Wijbrans, J., Ishizuka, O., He, H., Ramirez, A., Pfänder, J.A., Lopez-Martínez, M., Qiu, H. and Singer, B.S., 2021. Interpreting and reporting ^{40}Ar/^{39}Ar geochronologic data. Bulletin of the Geological Society of America, 133, 461-487. doi:10.1130/B35560.1

Söderlund, U. and Johansson, L., 2002. A simple way to extract baddeleyite (ZrO_2). Geochemistry, Geophysics, Geosystems, 3, 1-7.

Stacey, J.S. and Kramers, J.D., 1975. Approximation of terrestrial lead isotope evolution by a 2-stage model. Earth and Planetary Science Letters, 26, 207-221.

Steiger, R.H. and Jäger, E., 1977. Subcommission on geochronology: Convention on the use of decay constants in geo- and cosmochronology. Earth and Planetary Science Letters, 36, 359-362.

Stewart, K., Turner, S., Kelley, S., Hawkesworth, C.J., Kirstein, L. and Mantovani, M., 1996. 3-D, ^{40}Ar-^{39}Ar geochronology in the Paraná continental flood basalt province. Earth and Planetary Science Letters, 143, 95-109.

Stoenner, R.W., Schaeffer, O.A. and Katcoff, S., 1965. Half-lives of argon-37, argon-39, and argon-42. Science, 148, 1325-1328.

Sun, S. -s. and McDonough, W.F., 1989. Chemical and isotopic systematics of oceanic basalts: implications for mantle composition and processes. Geological Society of London, Special Publications, 42, 313-345. doi:10.1144/GSL.SP.1989.042.01.19

Svensen, H., Corfu, F., Polteau, S., Hammer, Ø. and Planke, S., 2012. Rapid magma emplacement in the Karoo Large Igneous Province. Earth and Planetary Science Letters, 325-326, 1-9.

Trumbull, R.B., Reid, D.L., De Beer, C.H. and Romer, R.L., 2007. Magmatism and continental breakup at the west margin of southern Africa: A geochemical comparison of dolerite dikes from northwestern Namibia and the Western Cape. South African Journal of Geology, 110, 477-502. doi:10.2113/gssajg.110.2-3.477

Weaver, B.L. and Tarney, J., 1984. Major and trace element composition of the continental lithosphere. Physics and Chemistry of the Earth, 15, 39-68.

White, R. and McKenzie, D., 1989. Magmatism at Rift Zones: The Generation of VolcanicContinental Margins. Journal of Geophysical Research, 94, 7685-7729.

Yamasaki, T., 2018. Contamination from mortars and mills during laboratory crushing and pulverizing. Bulletin of the Geological Survey of Japan, 69, 201-210.

Editorial handling: M.A. Elburg.